ACS APPLIED MATERIALS & INTERFACES

Research Article

www.acsami.org

First-Principles Analysis on the Catalytic Role of Additives in Low-Temperature Synthesis of Transition Metal Diborides Using Nanolaminates

Dongwoo Lee,[†] Joost J. Vlassak,*[,†] and Kejie Zhao*[,‡]

[†]John A. Paulson School of Engineering and Applied Sciences, Harvard University, Cambridge, Massachusetts 02138, United States
[‡]School of Mechanical Engineering, Purdue University, West Lafayette, Indiana 47906, United States

ABSTRACT: Carbon is known to significantly accelerate the formation reaction of zirconium diboride in reactive nanolaminates, although the detailed mechanism remains unclear. Here we investigate the catalytic effect of both C and N on the synthesis of ZrB_2 using a first-principles theoretical approach. We show that the strong interactions of C and N with Zr at the B/Zr interfaces of the nanolaminate enhance the solid-state amorphization of the Zr lattice. Amorphization of the Zr, in turn, accelerates intermixing of the constituent layers of the reactive nanolaminate. On the basis of these results we propose that the addition of elements with strong binding energies to transition metals may facilitate low-temperature synthesis of transition metal diborides using reactive nanolaminates.

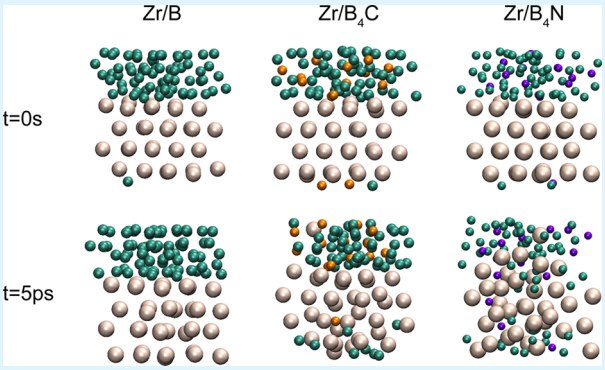

KEYWORDS: *reactive nanolaminate, amorphization, metal diborides, kinetics, first-principles*

1. INTRODUCTION

Transition metal diborides are metallic ceramics with a unique combination of properties, including extremely high melting points, outstanding chemical stability, high thermal conductivity, low electrical resistivity, low work function, and extreme hardness. This combination of properties has led to their use in low-temperature fuel cells,[1] in optoelectronics and microelectronics,[2−6] for hydrogen storage,[7] and as superhard materials.[8,9] Their high melting points, however, in addition to excellent chemical and mechanical stability require extreme processing conditions that limit their adoption in many applications.[2,9,10] Reactive nanolaminates (RNLs) that consist of alternating layers of a transition metal and boron provide a promising route to synthesize transition metal borides at relatively low temperatures and without contamination.[11−13] The formation of metal diborides using RNLs is typically a two-step process that starts with low-temperature intermixing and amorphization of the layers and concludes with the formation of a crystalline diboride compound at a more elevated temperature. The low reaction temperature is possible thanks to the formation of an intermediate amorphous phase that allows facile transport of B atoms[12,14]

Processing of transition metal diborides can be facilitated through use of additives. Carbon, for instance, is known as an effective sintering aid for diborides. Carbon promotes removal of surface oxides in ZrB_2 and limits grain growth, thus enhancing its sinterability. Recent experiments using nanocalorimetry have demonstrated that C also has a profound impact on the formation of ZrB_2 in RNLs. Kinetics studies of the intermixing of Zr and B and of the crystallization of amorphous ZrB_2 show that the activation energies for both processes are reduced by more than 20% when C is present in the RNL.[15] Carbon has a larger electronegativity difference with Zr (1.22) than B (0.71) and binds much more strongly with Zr. The accelerating effect of C runs counter to classical glass theory, which suggests that larger negative heats of mixing generally result in slower kinetic processes.[16−18] The kinetic role of carbon may be attributed to its role in the structural transformation that occurs at the Zr/B interface and results in the formation of the amorphous ZrB_2 compound—the strong bonding between Zr and C, in addition to the steep concentration gradients at the interface, enhances amorphization of the Zr lattice and thus facilitates the transport of B atoms. Since this process is associated with the Zr/B interface, we expect its effects to diminish as the thickness of the elemental layers in the RNLs increases and the overall process becomes more diffusion controlled, with a mechanism of nucleation and growth eventually taking over.

Here we perform a fundamental study of how additives such as C or N facilitate the synthesis of crystalline ZrB_2 using RNLs. The study is performed using first-principles computational methods within the framework of density functional theory (DFT). We start with a detailed examination of the energetics, bonding mechanism, and diffusion kinetics of B and C in bulk

Received: February 9, 2016
Accepted: April 12, 2016

DOI: 10.1021/acsami.6b01733
ACS Appl. Mater. Interfaces XXXX, XXX, XXX−XXX

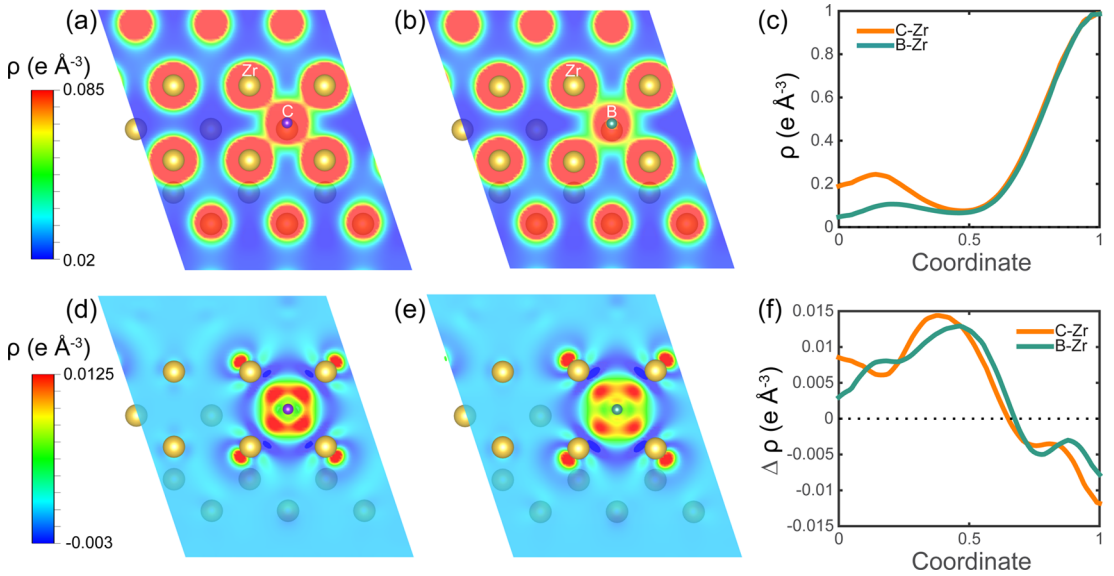

Figure 1. Valence electron charge density distribution on a (0 1 $\bar{1}$ 1) plane of the Zr lattice with an interstitial C or B atom: 2D map (a, b) and line profile between C or B and the nearest Zr atom (c). 2D maps of the charge density difference distribution in Zr with a C (d) or a B atom (e). (f) Line profile.

α-Zr. We show that interstitial C decreases the mobility of B in the Zr lattice and frustrates the amorphization of crystalline Zr. We then investigate the effects of C and N on the intermixing of Zr/BC_x or Zr/BN_y RNLs. We find that the addition of C or N to the B phase significantly enhances the amorphization of the crystalline Zr lattice at the interfaces and promotes transport of B through the amorphous layer. Evidently the effects of C and N are quite distinct for the bulk phase or the interface, even though in both cases these effects originate from the strong atomic bonding of C and N with Zr. On the basis of these results we propose that the addition of elements with strong binding energies to transition metals may be an effective method to facilitate the low-temperature synthesis of diborides. We compile a map of the heat of mixing of various transition metals with B, C, and N to guide the synthesis of diboride-based ceramics using RNLs.

2. COMPUTATIONAL METHODS

The first-principles calculations based on the DFT were carried out using the Vienna ab initio simulation package (VASP).[19] The projected-augmented-waves (PAW)[20] with the Perdew–Burke–Ernzerhof (PBE)[21] exchange-correlation potentials were adopted. For Zr, the valence states were treated using a Zr_sv ($4s^24p^65s^24d^2$) pseudopotential. B ($2s^22p$), C ($2s^22p^2$), and N ($2s^22p^3$) pseudopotentials were employed for B, C, and N, respectively. The cutoff energy for plane waves was set to 400 eV, and the forces converged to within 0.02 eV/Å. We used a 54-atom Zr supercell (3 × 3 × 3) and B and/or C interstitial atoms for the simulations of amorphization and interstitial diffusion. We utilized a 36-atom Zr supercell (3 × 3 × 2) and a 72-atom BC_xN_y amorphous layer in the AIMD simulations. For Brillouin zone sampling, 6 × 6 × 4, 6 × 6 × 4, and 1 × 1 × 1 k-point meshes in the Monkhorst–Pack scheme were employed for the amorphization, interstitial diffusion, and AIMD simulations, respectively. The AIMD simulations were performed at constant volume.

3. RESULTS AND DISCUSSION

We first study the electronic structure of crystalline α-Zr (space group $P6_3/mmc$, $a = b = 3.23$ Å, and $c = 5.17$ Å.[22,23]) with a B or C atom at an octahedral (Oct) interstitial site to understand the nature of the bond between Zr and B or C. The Oct site is energetically favorable for the insertion of both B and C.[14,15] Figures 1a and 1b show the distributions of the total valence electron charge densities on a (01$\bar{1}$1) plane of the Zr lattice with either an interstitial C or B atom. Figure 1c shows line profiles of the charge density distribution from the C or B atom to the nearest Zr atom. Close inspection of the graphs shows that atomic bonds of mixed covalent–ionic character are formed between the neighboring Zr atoms and the interstitial elements and that C forms a stronger bond with Zr than B. This is consistent with a prior study that revealed that the formation energy of a C interstitial at the Oct site is −1.53 eV, while the formation energy for a B interstitial is −0.53 eV.[14,15] Note that the stronger interaction makes the length of the bond between Zr and C (2.28 Å) shorter than that between Zr and B (2.34 Å).

To further explore the bond character of Zr–C and Zr–B we plot the charge density difference distributions on a (01$\bar{1}$1) plane of the Zr lattice with either a C or B interstitial in Figure 1d and 1e. The corresponding line profiles from the C or B atom to a neighboring Zr atom are shown in Figure 1f. Here the charge density difference $\Delta\rho$ is defined as $\Delta\rho = \rho_{nZr\text{-}I} - \rho_{Zr} - \rho_I$, where I represents either B or C. The charge densities $\rho_{nZr\text{-}I}$, ρ_{Zr}, and ρ_I represent the total charge densities of the Zr–I system (n Zr atoms and one I atom in the supercell), of the pure Zr system (n Zr atoms in the same positions as in the Zr–I system), and of an individual I atom, respectively. Both the Zr–B and the Zr–C bonds show an asymmetric distribution of $\Delta\rho$ with surplus electrons around the C or B atom and charge depletion on the side of the Zr atom, indicative of partial electron transfer from Zr to the interstitials. The charge depletion in Zr–C is larger than that of Zr–B because of the larger difference in electronegativity (electronegativities are 1.33 for Zr, 2.04 for B, and 2.55 for C, according to the Pauling scale).

Solid-state alloying of Zr–B in RNL occurs by amorphization of the Zr lattice and diffusion of B through the amorphous layer.[12] First, we investigate how B and C break Zr bonds and mediate the amorphization process and how the presence of C influences the transport of B in Zr single crystals. As shown in

DOI: 10.1021/acsami.6b01733
ACS Appl. Mater. Interfaces XXXX, XXX, XXX–XXX

Figure 2a, each Zr−Zr bond in the basal plane (dashed line) of α-Zr is surrounded by two octahedral sites (Oct_1 and Oct_2) and

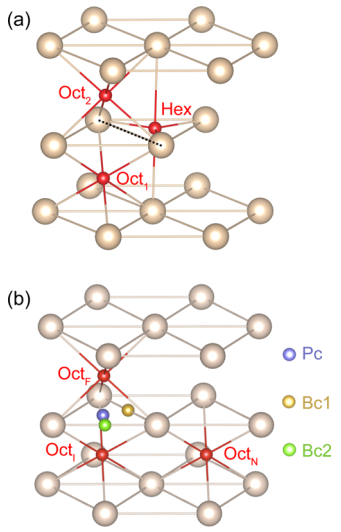

Figure 2. (a) Each Zr−Zr bond in the basal plane of α-Zr is surrounded by two Oct sites ($Oct_{1,2}$) and one Hex site. (b) Effect of an impurity atom at the neighboring Oct site (Oct_N) on the diffusion path of B from Oct (Oct_I) to Oct (Oct_F) along the c axis.

a hexahedral site (Hex), which are energetically favorable sites for the insertion of B or C. We do not consider unstable interstitial sites such as the tetrahedral site (Tet).[14,15,24,25] We place up to three C and/or B atoms at the three sites surrounding a given Zr bond and calculate the change in bond length between the Zr atoms. Table 1 lists the results. The

Table 1. Position of Impurity Atoms and the Resulting Zr−Zr Bond Length in the Zr Basal Plane

Oct_1	Oct_2	Hex	bond length (Å) (strain (%))
B	B		3.369 (4.01)
B	C		3.245 (0.19)
B		B	4.327 (33.58)
C		B	4.330 (33.68)
B		C	4.001 (23.53)
B	B	B	4.329 (33.65)
B	C	B	4.299 (32.73)
B	B	C	4.239 (30.87)

values between parentheses in the fourth column of the table are the strains of the Zr−Zr bond in the relaxed structure (the original bond length in α-Zr is 3.24 Å). It is clear from the table that all configurations in the table, except those where B or C occupy only the Oct sites in the Zr lattice, strain the Zr−Zr bond by more than 20%, significantly disrupting the bond. Interstitial C atoms generally stretch the Zr bonds less than B atoms at the same site. Clearly, C does not disrupt the Zr lattice structure as much as B, suggesting that the addition of C to bulk Zr does not promote amorphization as much as B.

In Figure 2b and Table 2, we illustrate the effect of a B or C atom at a neighboring Oct (Oct_N) site on the diffusion of B in the direction of the c axis (i.e., along the Oct_I−Oct_F path). We consider this diffusion path because as-deposited Zr in Zr/B_4C RNLs prepared by magnetron sputtering usually has a strong (0001) texture.[15] Oct_I−Oct_F transitions via a bond center (Bc_1), another bond center (Bc_2), and a plane center (Pc) sites

Table 2. Effect of Interstitial Atoms at Oct_N on the Diffusion Energy Barrier of B along the Oct_I−Oct_F Path

atom at Oct_N	B diffusion path	ΔE_s (eV)
none	Oct_I−Bc_1−Oct_F	1.60
none	Oct_I−Bc_2−Oct_F	1.60
none	Oct_I−Pc−Oct_F	2.80
C	Oct_I−Bc_1−Oct_F	1.84
C	Oct_I−Bc_2−Oct_F	1.93
C	Oct_I−Pc−Oct_F	2.66
B	Oct_I−Bc_1−Oct_F	1.66
B	Oct_I−Bc_2−Oct_F	1.88
B	Oct_I−Pc−Oct_F	2.60

are considered. The static energy difference (ΔE_s) between the initial position (Oct_I) and the saddle point (a B atom in Bc_1, Bc_2, or Pc) is taken as a measure of the diffusion energy barrier[14,15,25] for each trajectory. Table 2 lists the calculated ΔE_s for each diffusion path. It is evident that the Oct_I−Bc_1−Oct_F path always has the lowest energy barrier regardless of whether the Oct_N site is filled or the type of atom at the Oct_N site. It is also evident that filling the Oct_N site with C results in an increase in the energy barrier from 1.60−1.66 to 1.84 eV, indicating that C slows down diffusive transport of B. The Boltzmann factor, $\exp(-\Delta E_s/k_BT)$, where k_B represents the Boltzmann constant and T the absolute temperature, indicates that insertion of B at Oct_N reduces the probability of B diffusion along the Oct_I−Oct_F path by a factor of 2, while a C atom decreases the B diffusivity by more than an order of magnitude at 1000 K, the temperature where intermixing between B and Zr actively occurs.[12]

The above results indicate that addition of C to crystalline Zr decreases the mobility of B. We suggest that the increased energy barrier for B diffusion in bulk Zr in the presence of C is caused by the stronger interaction between Zr and C than between Zr and B—the C atom traps neighboring Zr atoms more effectively and restrains their displacements as B moves from one interstitial site to another. These observations clearly demonstrate that the enhanced reaction kinetics of Zr/B_4C RNLs is not due to enhanced B mobility in α-Zr, but is caused by processes associated with the amorphization of the crystalline Zr phase at the RNL interfaces.

To elucidate the amorphization process, we perform ab initio molecular dynamic simulations (AIMD) and explore the effects of C and N. A Zr/B multilayer structure (Figure 3a) is modeled by attaching an amorphous B layer of 72 atoms to the (0001) surface of a 3 × 3 × 2 α-Zr supercell (36 atoms). The amorphous B layer is created by first placing 10 B atoms at random positions in a space that has the same basal area as the Zr supercell and a height of approximately 48% of the thickness of the Zr supercell.[14] Additional B atoms are then inserted into this structure following a Delaunay triangulation (DT) analysis that identifies the largest voids in the structure. After inserting 10−12 B atoms, the amorphous structure is relaxed and the entire procedure is repeated until the structure contains 72 B atoms. Periodic boundary conditions are imposed on the a-B/Zr structure to model the multilayer geometry, and a final energy relaxation is performed to ensure that the structure is in a local energy minimum. This procedure ensures a better minimization of the interfacial mismatch compared to the case that B and Zr supercells are simply bonded. Zr/B_4C and the Zr/B_4N RNLs are constructed by randomly replacing a number of B atoms with C or N atoms to achieve the correct

DOI: 10.1021/acsami.6b01733
ACS Appl. Mater. Interfaces XXXX, XXX, XXX−XXX

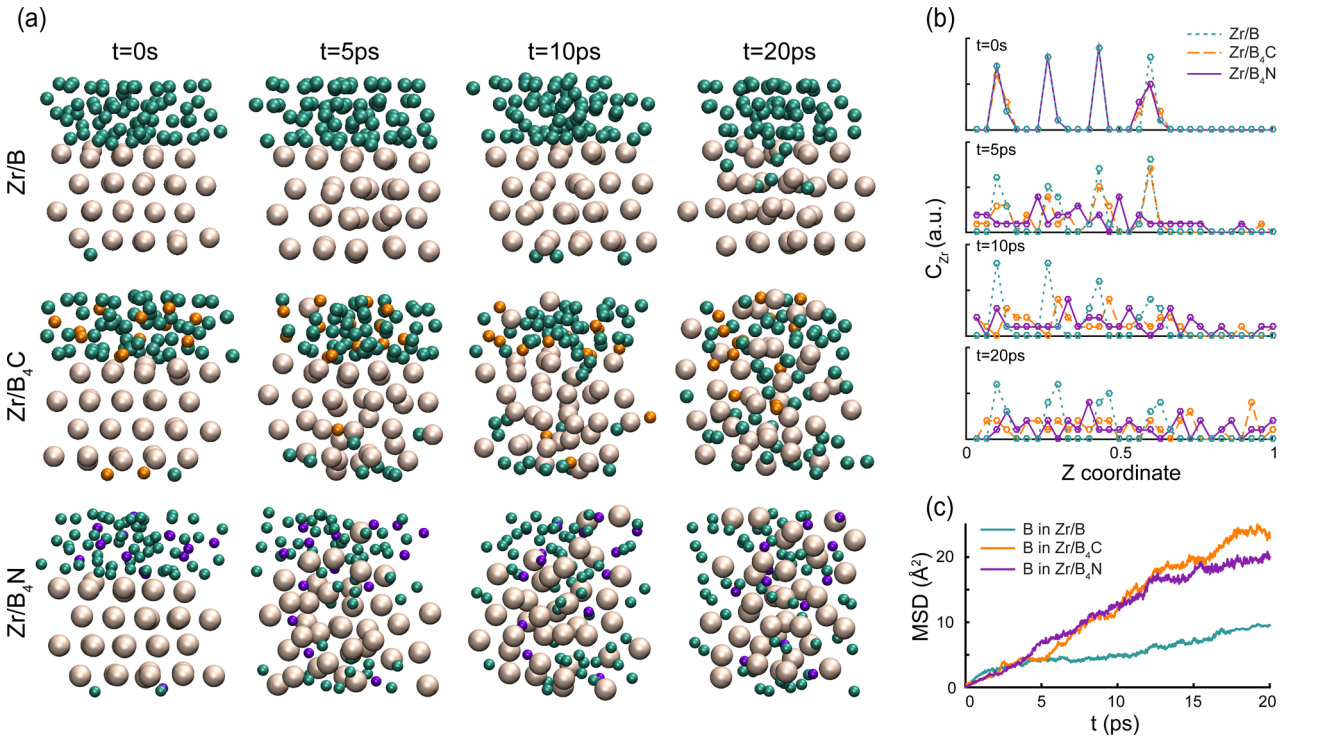

Figure 3. (a) Structural evolution of the Zr/B, Zr/B_4C, and Zr/B_4N RNLs upon annealing at 2000 K for 20 ps. Zr, B, C, and N atoms are represented by white, green, orange, and purple spheres, respectively. (b) Concentration profile of Zr vs the Z coordinate of the Zr/B (green, dotted), Zr/B_4C (orange, dashed), and Zr/B_4N (purple, solid) RNLs at different annealing times. (c) Mean square displacement (MSD) of B atoms.

stoichiometry. Ab initio molecular dynamics (AIMD) simulations are carried out at 2000 K to ensure that the reactions proceed sufficiently on the time scale of the simulations.[14] The supercells are allowed to dynamically equilibrate at each temperature for 10 000 time steps; each step corresponds to 2 fs.

Figure 3 shows the structural evolution of the RNLs, the Zr concentration (C_{Zr}) profile in the direction perpendicular to the RNL at different annealing times, and the mean square displacement (MSD) of the B atoms in each RNL. The value of the MSD is determined using MSD = $\langle |r_i(t) - r_i(0)|^2 \rangle$, where $r_i(t)$ is the position of atom i at time t, $r_i(0)$ is the position of atom i in the initial configuration, and $\langle \cdots \rangle$ represents an average over the ensemble of atoms. It is evident from Figure 3a and 3b that the Zr concentration is homogenized much more quickly in the Zr/B_4C and Zr/B_4N RNLs than in the Zr/B RNL. The mobility of the B atoms, as measured by the MSD, is shown in Figure 3c for the three RNLs. The addition of C and N to the amorphous B layer clearly enhances intermixing of the multilayered structure.

Figure 3 shows that amorphization of the Zr lattice occurs at the Zr/B_4(C, N) interface. The accelerated B transport is then a consequence of the enhanced amorphization of the Zr lattice at the Zr/B_4(C, N) interface, in good agreement with previous nanocalorimetry experiments.[12,14,15] We believe that the enhanced amorphization is caused by the stronger interaction between Zr and C or N than between Zr and B: C or N atoms at the interface distort the Zr lattice more effectively than B. The amorphous layer, in turn, enables faster B diffusion because of its larger free volume. As shown in Figure 3a, Zr is progressively amorphized as this interface/reaction front propagates until intermixing is complete. These kinetic processes are driven by the steep concentration gradient at the interface between both phases. This qualitative understanding explains the enhanced reactivity of Zr/B RNLs in the presence of C observed in nanocalorimetry experiments.[12,15]

Our results suggest that any dopant atoms in the amorphous layers of the RNLs with a strong affinity for Zr and similar in size to B may enhance the amorphization of the Zr lattice and promote intermixing of the constituent layers. From the above results, one would expect N to have a stronger effect than C because the heat of mixing of the Zr−N bond is −233 kJ/mol, compared to −131 kJ/mol for Zr−C[26] (Figure 4b). The larger negative heat of mixing in Zr−N is attributed to the larger difference in electronegativity (Figure 4a). Figure 3a−c shows a comparison of the structural evolution and B mobility for Zr/B_4C and Zr/B_4N RNLs. As expected, amorphization in the Zr/B_4N structure occurs earlier than in Zr/B_4C, achieving faster homogenization of the composition: the Zr/B_4N RNL is almost fully homogenized after 5 ps, while the Zr/B_4C RNL still has an unreacted Zr layer. As a result, the MSD of the B atoms in the Zr/B_4N RNL (6.3 A^2) is larger than in the Zr/B_4C RNL (3.6 A^2) at 5 ps. Note that for Zr/B RNLs with various configurations of the amorphous B layer the scatter in MSD is smaller than 1.5 A^2 over this time period. After 10 ps, the MSD of the B atoms in Zr/B_4N is slightly smaller than in Zr/B_4C—the MSD curves at this time represent the mobility of B atoms in the amorphous ZrB_xC_y and ZrB_xN_y phases in the absence of sharp concentration gradients. In homogeneous solutions, N decreases the mobility of B even more than C. This behavior is consistent with the glass theory—in a homogeneous solid solution, atoms with larger negative heat of mixing typically have lower mobility, thus promoting the glass forming ability of the solution.[16−18]

It is noteworthy that transition metals (TMs) that form crystalline diborides, such as Sc, Ti, V, Cr, Mn, Fe, Y, Nb, and

DOI: 10.1021/acsami.6b01733
ACS Appl. Mater. Interfaces XXXX, XXX, XXX−XXX

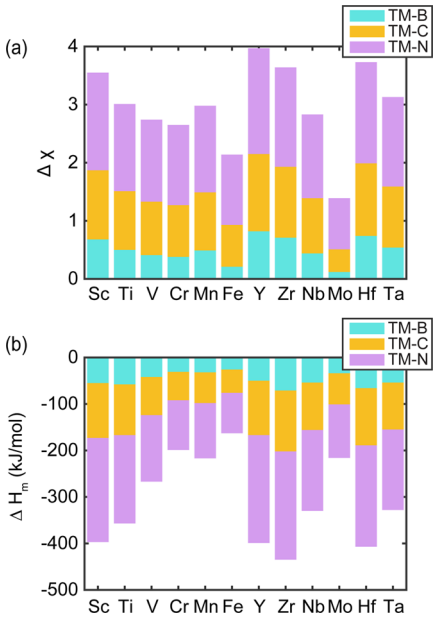

Figure 4. (a) Differences between transition metals (TMs) and B, C, or N atoms in (a) electronegativity and (b) heat of mixing. Data taken from refs 26 and 27.

Mo, also have the largest negative heats of mixing and the largest differences in electronegativity with N, followed by C, and then by B,[26,27] as shown in Figure 4. We propose that the addition of C and/or N to the amorphous B layer will enhance the processability of transition diborides using TM/B RNLs.

4. CONCLUSIONS

In summary, we employed a first-principles approach to investigate the catalytic role of additives in the low-temperature synthesis of metal diborides using RNLs. The beneficial effect of C and N on the synthesis of ZrB_2 is attributed to the enhanced amorphization of the Zr and the enhanced intermixing of the constituent layers driven by the steep concentration gradient at the reaction front. While the strong interaction between C/N and Zr reduces the mobility of B in bulk Zr and the amorphous phase, it facilitates the interfacial processes responsible for the amorphization. We suggest that dopants with a strong binding energy with transition metals may also facilitate the synthesis of diboride-based ceramics using RNLs. The findings are in agreement with recent nanocalorimetry experiments and provide important guidance for the synthesis of transition metal diborides.

AUTHOR INFORMATION

Corresponding Authors

*E-mail: Vlassak@seas.harvard.edu.
*E-mail: kjzhao@purdue.edu.

Notes

The authors declare no competing financial interest.

ACKNOWLEDGMENTS

This work was supported by the Air Force Office of Scientific Research under Grant No. FA9550-12-1-0098 and by the National Science Foundation under Grant No. DMR-1435820. It was performed in part at the Center for Nanoscale Systems at Harvard University, which is supported by the National Science Foundation under Award No. ECS-0335765, and at the Materials Research Science and Engineering Center at Harvard University, which is supported by the National Science Foundation under Award No. DMR-14-20570. K.Z. is grateful for the start-up funding provided by Purdue University.

REFERENCES

(1) Wu, P.; Lv, H. F.; Peng, T.; He, D. P.; Mu, S. C. Nano Conductive Ceramic Wedged Graphene Composites as Highly Efficient Metal Supports for Oxygen Reduction. *Sci. Rep.* **2014**, *4*, 3968.
(2) Carenco, S.; Portehault, D.; Boissiere, C.; Mezailles, N.; Sanchez, C. Nanoscaled Metal Borides and Phosphides: Recent Developments and Perspectives. *Chem. Rev.* **2013**, *113* (10), 7981−8065.
(3) Liu, R.; Bell, A.; Ponce, F. A.; Kamiyama, S.; Amano, H.; Akasaki, I. Atomic arrangement at the AlN/ZrB_2 interface. *Appl. Phys. Lett.* **2002**, *81* (17), 3182−3184.
(4) Suda, J.; Matsunami, H. Heteroepitaxial Growth of Group-III Nitrides on Lattice-Matched Metal Boride ZrB_2 (0001) by Molecular Beam Epitaxy. *J. Cryst. Growth* **2002**, *237-239*, 1114−1117.
(5) Tolle, J.; Roucka, R.; Tsong, I. S. T.; Ritter, C.; Crozier, P. A.; Chizmeshya, A. V. G.; Kouvetakis, J. Epitaxial Growth of Group III Nitrides on Silicon Substrates via a Reflective Lattice-Matched Zirconium Diboride Buffer Layer. *Appl. Phys. Lett.* **2003**, *82* (15), 2398−2400.
(6) Yamada-Takamura, Y.; Wang, Z. T.; Fujikawa, Y.; Sakurai, T.; Xue, Q. K.; Tolle, J.; Liu, P. L.; Chizmeshya, A. V. G.; Kouvetakis, J.; Tsong, I. S. T. Surface and Interface Studies of GaN Epitaxy on Si(111) via ZrB_2 Buffer Layers. *Phys. Rev. Lett.* **2005**, *95* (26), 266105.
(7) Meng, S.; Kaxiras, E.; Zhang, Z. Y. Metal-Diboride Nanotubes as High-Capacity Hydrogen Storage Media. *Nano Lett.* **2007**, *7* (3), 663−667.
(8) Gu, Q.; Krauss, G.; Steurer, W. Transition Metal Borides: Superhard versus Ultra-Incompressible. *Adv. Mater.* **2008**, *20* (19), 3620−3626.
(9) Chung, H. Y.; Weinberger, M. B.; Levine, J. B.; Kavner, A.; Yang, J. M.; Tolbert, S. H.; Kaner, R. B. Synthesis of Ultra-Incompressible Superhard Rhenium Diboride at Ambient Pressure. *Science* **2007**, *316* (5823), 436−439.
(10) Fahrenholtz, W. G.; Hilmas, G. E.; Talmy, I. G.; Zaykoski, J. A. Refractory Diborides of Zirconium and Hafnium. *J. Am. Ceram. Soc.* **2007**, *90* (5), 1347−1364.
(11) Lee, D.; Sim, G. D.; Xiao, K. C.; Choi, Y. S.; Vlassak, J. J. Scanning AC Nanocalorimetry Study of Zr/B Reactive Multilayers. *J. Appl. Phys.* **2013**, *114* (21), 214902.
(12) Lee, D.; Sim, G. D.; Xiao, K. C.; Vlassak, J. J. Low-Temperature Synthesis of Ultra-High-Temperature Coatings of ZrB_2 Using Reactive Multilayers. *J. Phys. Chem. C* **2014**, *118* (36), 21192−21198.
(13) Reeves, R. V.; Rodriguez, M. A.; Jones, E. D.; Adams, D. P. Condensed-Phase and Oxidation Reaction Behavior of Ti/2B Foils in Varied Gaseous Environments. *J. Phys. Chem. C* **2012**, *116* (33), 17904−17912.
(14) Lee, D.; Vlassak, J. J.; Zhao, K. First-Principles Theoretical Studies and Nanocalorimetry Experiments on Solid-State Alloying of Zr−B. *Nano Lett.* **2015**, *15* (10), 6553−6558.
(15) Lee, D.; Sim, G.-D.; Zhao, K.; Vlassak, J. J. Kinetic Role of Carbon in Solid-State Synthesis of Zirconium Diboride Using Nano-Laminates: Nanocalorimetry Experiments and First-Principles Calculations. *Nano Lett.* **2015**, *15* (12), 8266−8270.
(16) Johnson, W. L. Thermodynamic and Kinetic Aspects of the Crystal to Glass Transformation in Metallic Materials. *Prog. Mater. Sci.* **1986**, *30* (2), 81−134.
(17) Greer, A. L. Metallic Glasses. *Science* **1995**, *267* (5206), 1947−1953.
(18) Schroers, J. Bulk Metallic Glasses. *Phys. Today* **2013**, *66* (2), 32−37.
(19) Kresse, G.; Furthmuller, J. Efficient Iterative Schemes for Ab Initio Total-Energy Calculations Using a Plane-Wave Basis Set. *Phys. Rev. B: Condens. Matter Mater. Phys.* **1996**, *54* (16), 11169−11186.

DOI: 10.1021/acsami.6b01733
ACS Appl. Mater. Interfaces XXXX, XXX, XXX−XXX

(20) Kresse, G.; Joubert, D. From Ultrasoft Pseudopotentials to the Projector Augmented-Wave Method. *Phys. Rev. B: Condens. Matter Mater. Phys.* **1999**, *59* (3), 1758−1775.
(21) Perdew, J. P.; Burke, K.; Ernzerhof, M. Generalized Gradient Approximation Made Simple. *Phys. Rev. Lett.* **1996**, *77* (18), 3865−3868.
(22) Willaime, F. Ab Initio Study of Self-Interstitials in Hcp-Zr. *J. Nucl. Mater.* **2003**, *323* (2−3), 205−212.
(23) Samolyuk, G. D.; Barashev, A. V.; Golubov, S. I.; Osetsky, Y. N.; Stoller, R. E. Analysis of the Anisotropy of Point Defect Diffusion in Hcp Zr. *Acta Mater.* **2014**, *78*, 173−180.
(24) Hennig, R. G.; Trinkle, D. R.; Bouchet, J.; Srinivasan, S. G.; Albers, R. C.; Wilkins, J. W. Impurities Block the Alpha to Omega Martensitic Transformation in Titanium. *Nat. Mater.* **2005**, *4* (2), 129−133.
(25) Wu, H. H.; Trinkle, D. R. Direct Diffusion Through Interpenetrating Networks: Oxygen in Titanium. *Phys. Rev. Lett.* **2011**, *107* (4), 045504.
(26) Takeuchi, A.; Inoue, A. Classification of Bulk Metallic Glasses by Atomic Size Difference, Heat of Mixing and Period of Constituent Elements and Its Application to Characterization of the Main Alloying Element. *Mater. Trans.* **2005**, *46* (12), 2817−2829.
(27) Haynes, W. M. *CRC Handbook of Chemistry and Physics*, 92nd ed; CRC Press: Boca Raton, FL, 2011; pp 9−99.

DOI: 10.1021/acsami.6b01733
ACS Appl. Mater. Interfaces XXXX, XXX, XXX−XXX